



Analysis of laminar flow and heat transfer in an interrupted microchannel heat sink with different shaped ribs

Wei Wang^{1,2} · Yongji Li¹ · Yanning Zhang¹ · Bingxi Li¹ · Bengt Sundén³

Received: 1 September 2019 / Accepted: 4 December 2019 / Published online: 18 December 2019
© The Author(s) 2019

Abstract

A numerical study was conducted to investigate the mechanism of laminar flow and heat transfer enhancement in an interrupted microchannel heat sink (IMCHS) with different shaped ribs at Reynolds number ranging from 100 to 900. The global flow features, heat transfer and friction for IMCHS with no ribs, rectangle ribs, triangle ribs and trapezoid ribs are detailed compared. The results show that the local heat transfer and friction performance of IMCHS with ribs show significant increase at the windward side of the ribs. Additionally, the smaller the chamfer of ribs, the larger average heat transfer and friction performance. For IMCHS with rectangle ribs, the maximum increment of Nu and f can reach to 1.81 and 2.59, respectively. Concerning the overall heat transfer performance (PEC), the trapezoid ribs show the best behavior with $PEC = 1.65$ – 1.38 at $Re = 100$ – 900 .

Keywords Interrupted microchannel heat sink · Different rib shapes · Numerical simulation · Overall heat transfer performance

List of symbols

C_p	Specific heat ($J\ kg^{-1}\ K^{-1}$)
D_e	Hydraulic diameter (mm)
f	Darcy friction factor
h	Heat transfer coefficient ($W\ m^{-2}\ K^{-1}$)
L	Length (m)
Nu	Nusselt number
P	Pressure (Pa)
PEC	Overall heat transfer performance
Pr	Prandtl number
q	Average heat flux ($W\ m^{-2}$)
Re	Reynolds number
T	Temperature (K)
u	Velocity ($m\ s^{-1}$)

x, y, z	Three coordinates shown in Fig. 1
ΔP	Pressure drop (Pa)

Greek letters

λ	Thermal conductivity ($W\ m^{-1}\ K^{-1}$)
μ	Dynamic viscosity ($kg\ m^{-1}\ s^{-1}$)
ρ	Density ($kg\ m^{-3}$)

Subscripts

ave	Average value
f	Fluid
i, j, k	Directions of the coordinate system
in	Inlet
local	Local value
out	Outlet
w	Wall
0	Reference value

✉ Bingxi Li
libx@hit.edu.cn

✉ Bengt Sundén
bengt.sunden@energy.lth.se

¹ School of Energy Science and Engineering, Harbin Institute of Technology, Harbin 150001, China

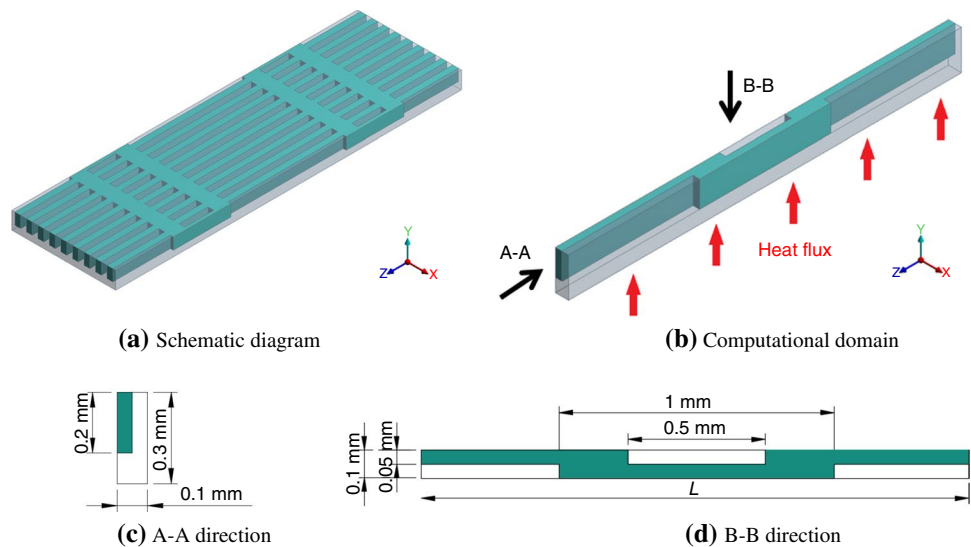
² School of Environment, Harbin Institute of Technology, Harbin 150001, China

³ Department of Energy Sciences, Lund University, 22100 Lund, Sweden

Introduction

With the development of the electronics industry, the power of electronic components has gradually increased. Thus, more effective heat dissipation methods were urgently needed. Various kinds of enhanced heat sinks have been studied recently such as radial heat sink with fins used on high-power LED lightings [1], cooling of electronics using phase change material [2] and nanofluids [3–5]-based heat

Fig. 1 Schematic diagram and computational domain of IMCHS with rectangular rib



sinks, water-cooling in smooth microchannel heat sinks with obstructions [6].

The forced convection heat transfer in microchannels with liquid has higher efficiency and is easier for utilization than other methods. Some scholars used various kinds of nanofluids as the heat transfer fluid in microchannels [7–10]. Thermal and hydrodynamic performance of an MCHS with carbon nanotube nanofluids was investigated by Normah et al. [10]. The results showed that the nanotube nanofluid with lignin as the surfactant performed better thermally and hydrodynamically, due to lower viscosity at high carbon nanotube concentration compared to the nanotube nanofluid with sodium polycarboxylate surfactant. Different kinds of nanofluids and drop-shaped micropin fins distribution density of MCHS were numerically analyzed by Keshavarz et al. [11]. The results showed that using drop-shaped fins instead of circular-shaped fins increases the outlet temperature by 0.6% and decreases the pumping work by 13.3%. Moreover, using Al_2O_3 -water nanofluid instead of pure water results in outlet temperature and pump work increase of 0.4% and 1%, respectively. Bahiraei and Heshmatian [12] using the graphene-silver hybrid nanofluid as heat transfer fluid in two new microchannel heat sinks. The results shown that the heat sink with more path changes and nanofluids can be promising options to be utilized in electronics cooling regarding both first and second laws of thermodynamics.

But the nanofluids are easily settled for long times operations, which is a disaster for microchannels. Therefore, more studies are still concerned about water as the heat transfer fluid. Wang et al. [13] studied the influence of geometric shape and parameters of the channel's cross section on the flow and heat transfer performance of a microchannel heat sink (MCHS) with water as the coolant. Among three kinds of microchannel, the rectangle has the lowest thermal resistance, followed by trapezoid and triangle microchannel. The

channel number also affects the thermal resistance and pressure drop and has an optimum range. Ahmed and Ahmed [14] numerically studied the laminar water flow and forced convection heat transfer characteristics in MCHS with different shaped cavities. The results showed that the trapezoidal groove with groove tip length ratio of 0.5, groove depth ratio of 0.4, groove pitch ratio of 3.334, grooves orientation ratio of 0 and $\text{Re} = 100$ is the optimum thermal design for grooved microchannel heat sink with Nu enhancement of 51.59% and friction factor improved of 2.35%. Xie et al. [15] parametrically studied the thermal performance of MCHS with internal vertical Y-shaped bifurcations. It is found that the thermal performance of microchannel heat sink with internal Y-shaped bifurcations is much better than that of the traditional rectangular microchannel. The longest and larger arm angle of internal Y-shaped bifurcation microchannel results in the best thermal performance. Chai et al. [16] compared a straight microchannel, interrupted microchannel heat sink (IMCHS) and IMCHS with rectangular rib. It is found that the interrupted microchannel with ribs is suitable to the operating condition of $\text{Re} < 600$, and for $\text{Re} > 600$, the interrupted microchannel without ribs is considered better. Wong and Lee [17] investigated the IMCHS with different geometric parameters of triangular ribs. The results of thermal enhancement factor reveal an optimum geometrical parameters for the triangular rib with width = 100 μm , length = 400 μm and height = 120 μm for about Re of 500, yielding 43% enhancement relative to non-interrupted rectangular microchannel heat sink at equal pumping power.

From all above literatures, heat transfer enhancement by the IMCHS with ribs was confirmed. Most of them only concerned the average characteristics of heat transfer and friction, and only a few works concerned the global performance. In this work, the fully developed laminar flow of IMCHS with ribs is numerically investigated. The

velocity vectors, local Nusselt number and local friction factor are combined and analyzed to explore the mechanism of enhanced heat transfer. Four kinds of IMCHS with no ribs (NR), rectangle ribs (R1), triangle ribs (R2) and trapezoid ribs (R3) are compared, to discuss the effect of rib chamfer. The average Nusselt number (Nu), friction factor (f) and overall heat transfer performance (PEC) are also presented in details.

Mathematical approach

Geometry and grids

The schematic diagram and computational domain of the interrupted microchannel heat sink (IMCHS) with rectangular ribs are shown in Fig. 1. In order to save the computational efforts, the half of a unit IMCHS is numerically analyzed with symmetry boundary conditions at the two $y-z$ surfaces. The structural parameters of the IMCHS with ribs are depicted in Fig. 1c, d.

Four kinds of IMCHSs are compared in this work. The geometric models are shown in Fig. 2 [18]. These are the IMCHS without ribs (IMCHS-NR), the IMCHS with rectangle-shaped ribs (IMCHS-R1), the IMCHS with triangle-shaped ribs (IMCHS-R2) and the IMCHS with trapezoid-shaped ribs (IMCHS-R3), from (a) to (d). The angle of the rib chamfers is both 45° for IMCHS-R2 and IMCHS-R3.

Unstructured tetrahedral grids are employed in the computational domain with the grid refinements at the boundary layers, as shown in Fig. 3. A grid independence study is conducted for the IMCHS-R1 at $Re = 900$. The corresponding results are presented in Fig. 4, the Nu and f show good stability for mesh above 35 millions, with the error being $< 2\%$ compared with the 45 millions grids. Hence, the mesh total number of 35 millions is performed in this study.

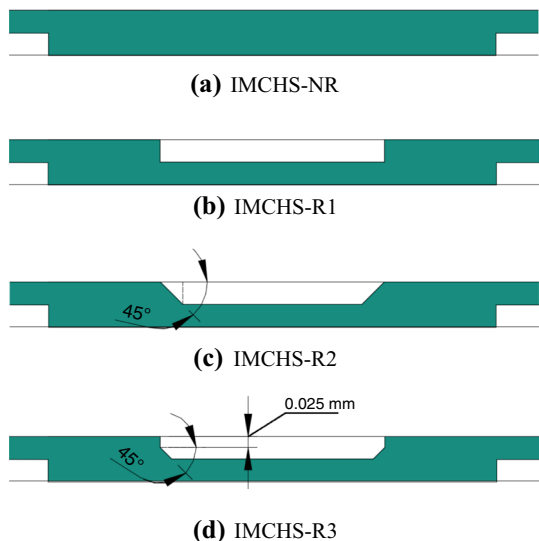
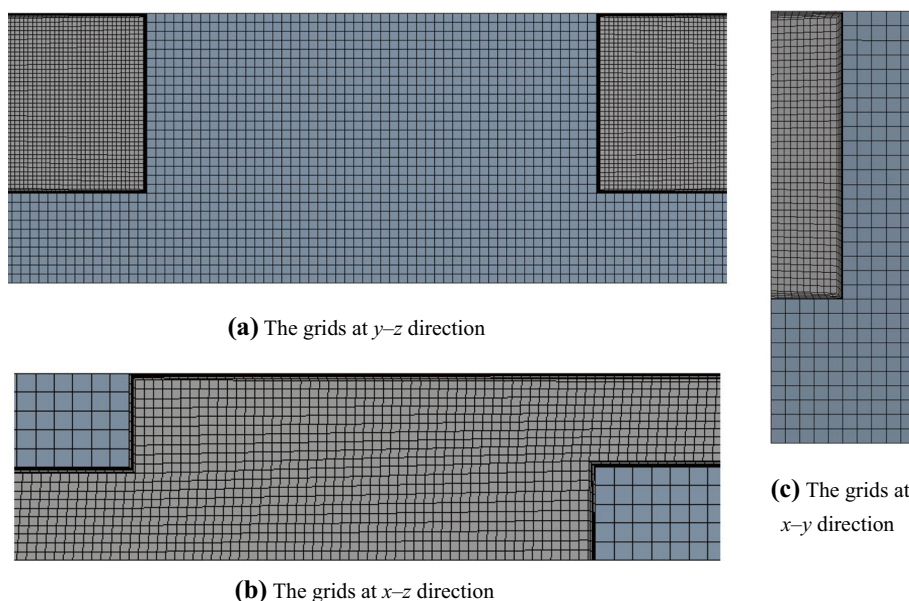


Fig. 2 Four kinds of IMCHS with different shaped ribs

Governing equations

The following assumptions are adopted in this work: (a) the body force is neglected; (b) the fluid flow is assumed to be steady, laminar and incompressible; and (c) the

Fig. 3 Computational grids used in the numerical simulations



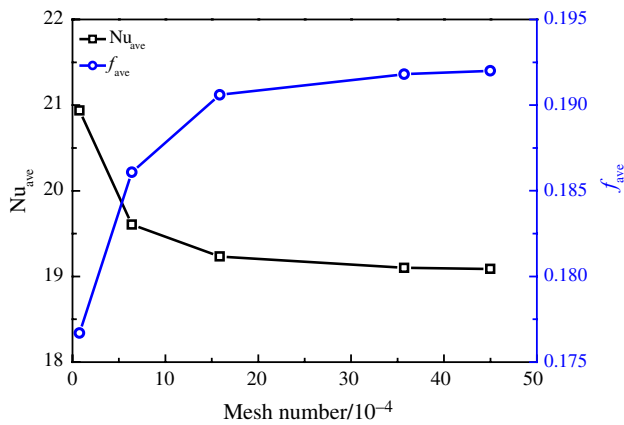


Fig. 4 Mesh independence test for IMCHS-R1 (Re = 900)

Table 1 Thermo-physical properties of silicon [16]

Properties	Unit	Variable
Density (ρ)	kg m ⁻³	2330
Specific heat (Cp)	J kg ⁻¹ K ⁻¹	700
Thermal conductivity (λ)	W m ⁻¹ K ⁻¹	150

thermo-physical properties of the solid (silicon) are considered to be same as shown in Table 1. The fluid (water) properties vary with temperature are shown in Table 2 [16], and the thermal conductivity and viscosity are fitted with the data.

Based on the above assumptions, the governing equations of continuity, momentum and energy for laminar heat transfer flow in microchannels are as follows [19]:

The continuity equation:

$$\frac{\partial}{\partial x_i} (\rho u_i) = 0 \tag{1}$$

The momentum equation:

$$\frac{\partial}{\partial x_i} (\rho_f u_i u_j) = -\frac{\partial p}{\partial x_j} + \frac{\partial}{\partial x_i} \left[\mu_f \left(\frac{\partial u_i}{\partial x_j} + \frac{\partial u_j}{\partial x_i} \right) \right] \tag{2}$$

Energy equation (fluid):

$$\frac{\partial}{\partial x_i} (\rho_f c_{pf} u_i T) = \frac{\partial}{\partial x_i} \left(\lambda_f \frac{\partial T}{\partial x_i} \right) + \mu_f \left[2 \left(\frac{\partial u_i}{\partial x_i} \right)^2 + \left(\frac{\partial u_i}{\partial x_j} + \frac{\partial u_j}{\partial x_i} \right)^2 \right] \tag{3}$$

Energy equation (solid):

$$\frac{\partial}{\partial x_i} \left(\lambda_s \frac{\partial T}{\partial x_i} \right) = 0 \tag{4}$$

Numerical procedure

Numerical steady-state simulations are used to solve the laminar flow and heat transfer in the microchannels. The semi-implicit algorithm for pressure-linked equations (SIMPLE) is used to couple the velocity and pressure fields. The second-order upwind scheme is used for the energy and momentum equations. Convergence criteria scaled residuals for continuity, momentum and energy equations should be < 10⁻⁴, 10⁻⁵ and 10⁻⁶, respectively [20].

Boundary conditions

Inlet condition fully developed velocity and temperature profiles as inlet conditions, and the fixed average velocity (u_{in}) and average temperature ($T_{in} = 293$ K);

Outlet condition pressure outlet ($P_{out} = 0.103$ MPa).

Wall condition the bottom wall has a fixed heat flux condition ($q_w = 1.24$ MW m⁻²), the two y - z surfaces are symmetry boundaries, the wall interfaces with the fluid are no slip boundaries, and other walls than the bottom wall are adiabatic.

Data reduction

The Nusselt number and Darcy friction factor are employed to represent the heat transfer and flow resistance [21].

$$Nu = \frac{hDe}{\lambda} \tag{5}$$

$$h = \frac{q}{T_{wall} - 0.5(T_{in} + T_{out})} \tag{6}$$

Table 2 Thermo-physical properties of water [16]

Properties	Unit	293/K	303/K	313/K	323/K
Density (ρ)	kg m ⁻³	998.2	995.7	992.2	988.1
Specific heat (Cp)	J kg ⁻¹ K ⁻¹	4183	4174	4174	4174
Thermal conductivity (λ)	W m ⁻¹ K ⁻¹	0.599	0.618	0.635	0.648
Dynamic viscosity (μ)	kg m ⁻¹ s ⁻¹	1.00E-3	8.015E-4	6.533E-4	5.494E-4
Pr	-	7.01	5.41	4.29	3.54

$$f = \frac{2\Delta PDe}{\rho Lu^2} \tag{7}$$

where De is hydraulic diameter, h is convective heat transfer coefficient, λ is the fluid thermal conductivity, L is the channel length, u is the mean fluid velocity and ΔP is the pressure drop between the inlet and outlet.

The overall heat transfer performance (PEC) [22] is employed to compare the enhanced heat transfer performance and increased flow resistance for the IMCHSs.

$$PEC = \frac{Nu/Nu_0}{(f/f_0)^{1/3}} \tag{8}$$

where the subscript “0” denotes interrupted microchannel without ribs. If $PEC > 1$, the enhanced overall heat transfer performance is superior compared to the IMCHS-NR [23].

Results and discussion

Validation

In order to test the accuracy of the numerical method, the simulation results are compared with the experimental data [16] in an interrupted microchannel heat sink with rectangular ribs in transverse microchambers, with width ratio and length ratio both equal to 0.5. As illustrated in Fig. 5, the comparisons show good agreement between the numerical results and experimental data, and the maximum error is less than $\pm 10\%$.

Global velocity, heat transfer and friction performance

Global distributions of velocity fields and vectors (middle surface, $Re = 500$) for IMCHS with different shaped ribs are shown in Fig. 6. It can be seen that the velocity contours of IMCHS-NR show a big low-speed region at the microchambers which is useless for improvement in heat transfer [24]. The velocity contours of IMCHS with ribs show complex flow features, two back flow region are produced at the two sudden expansion regions, and the fluid is speeding up at the rib region and increases the contact area between the fluid and solid. The triangle-shaped rib (R2) and trapezoid-shaped rib (R3) are studied to reduce the dead zone of the fluid flow compared to the rectangle-shaped rib (R1). The velocity contours show that the boundary layer thickness at the rib surface is $R1 > R3 > R2$. The acceleration effect is $R1 > R3 > R2$, as well.

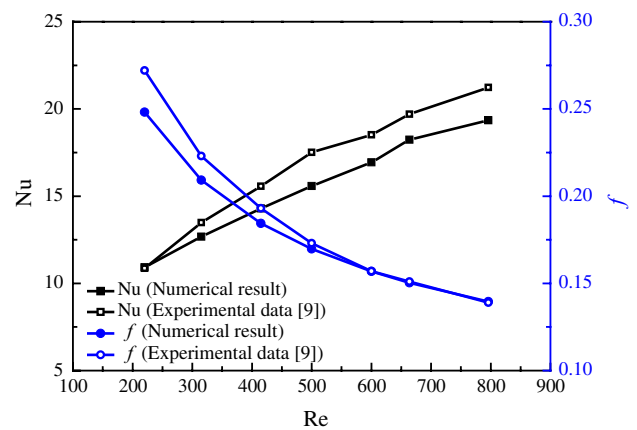


Fig. 5 Comparison of the numerical results and experimental data of IMCHS

The temperature fields distribution for IMCHS with different shaped ribs (bottom surface, $Re = 500$) are shown in Fig. 7. It can be seen that the fluid temperature is increased with the decrease in velocity. For IMCHS-NR, the flow temperature at whole interrupted region maintains higher degree. However, the fluid temperature at the second back flow region is much lower than it at the first back flow region for IMCHS with ribs. And the fluid temperature at first back flow region is nearly the same for the three kinds of ribs, but the fluid temperature is $R2 > R3 > R1$ at the second back flow region. It indicates that the rib shapes have little effect on the first back flow, but is very important for the second back flow production.

The local Nusselt number (Nu_{local}) and friction factor (f_{local}) [25] for IMCHS with different shaped ribs (bottom surface, $Re = 500$) are shown in Figs. 8 and 9. The Nu_{local} and f_{local} both show an obvious increase at the fluid acceleration area. It can be seen that the IMCHS-NR has no effect on the improvement in heat transfer and friction factor. The IMCHSs with three kinds of ribs show significant increase in Nu_{local} and f_{local} at the sudden converging channel, which mainly is caused by the flow impinging to the walls. With the increase in rib chamfer ($R2 > R3 > R1$), the Nu_{local} and f_{local} at the windward side of the rib are gradually decreased. On the other hand, for the leeside of the rib, the Nu_{local} and f_{local} are also decreasing with the increase in rib chamfer.

Average heat transfer and friction performance

The average Nusselt number (Nu_{ave}) and friction factor (f_{ave}) versus Re for IMCHS with different shaped ribs are shown in Figs. 10 and 11. The Nu_{ave} increases with the increase in Re , with the growth rate gradually decreasing.

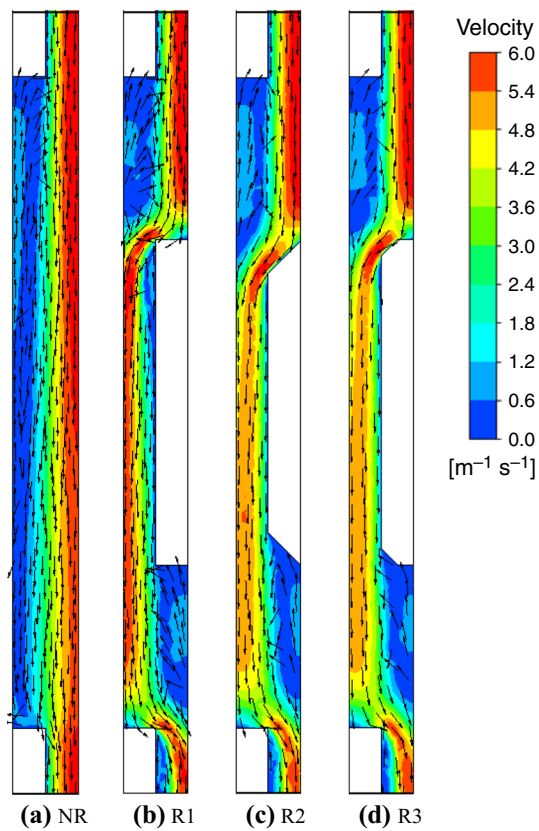


Fig. 6 Velocity contours and vectors for the IMCHS with different shaped ribs (middle surface, $Re = 500$)

The f_{ave} sharply decreases from $Re = 100$ to $Re = 300$, then declining rate is moderate, and the f_{ave} value tends to be constant. The IMCHS with ribs show an obvious increase in Nu_{ave} and f_{ave} compared to the IMCHS-NR. The enhancement of Nu_{ave} for R1, R2 and R3 to NR are 1.72–1.81, 1.64–1.67 and 1.68–1.73 times, respectively, and the enhancement of f_{ave} for R1, R2 and R3 to NR are 1.12–2.59, 1.04–1.85 and 1.07–1.97 times with Reynolds number in the range of 100 to 900, respectively. The increase ratios of Nu_{ave} and f_{ave} are $R1 > R3 > R2$, but the flow resistance for R1 shows deterioration.

The average PEC for IMCHS with three kinds of ribs versus Re are shown in Fig. 12. The PECs are decreased with the increase in Re , because the Nu/Nu_0 is decreased and the ff_0 is increased with the increase of Re . It indicates that the enhanced heat transfer technique is more meaningful for low Re . For the whole considered Re range, the PECs of the IMCHS with three kinds of ribs are all above 1.3; it means the improved heat transfer is superior to the energy losses caused by pressure drop. The trapezoid rib (R3) shows the best behavior in the whole considered Re range. The rectangle rib (R1) is superior to the triangle rib (R2) at the low Re range ($Re < 500$), and the R2 is superior to R1 at the high Re range ($Re > 500$). This is because the

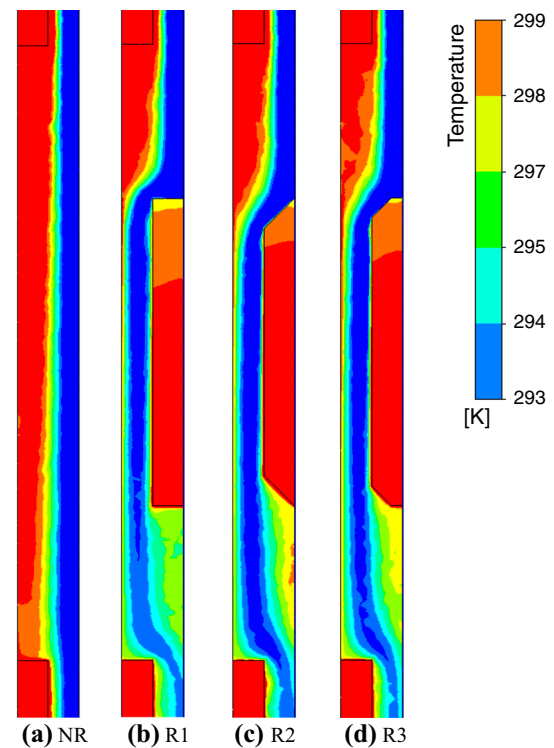


Fig. 7 Temperature distribution for the IMCHS with different shaped ribs (bottom surface, $Re = 500$)

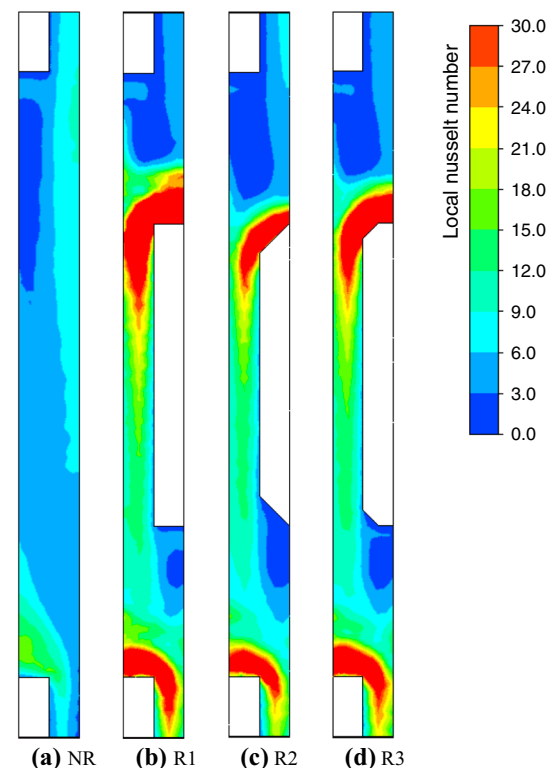


Fig. 8 Local Nusselt number for the IMCHS with different shaped ribs (bottom surface, $Re = 500$)

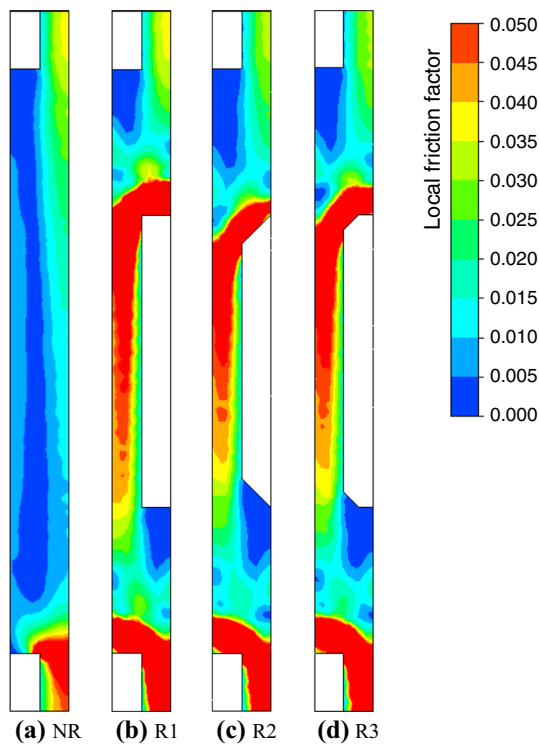


Fig. 9 Local friction factor for the IMCHS with different shaped ribs (bottom surface, $Re = 500$)

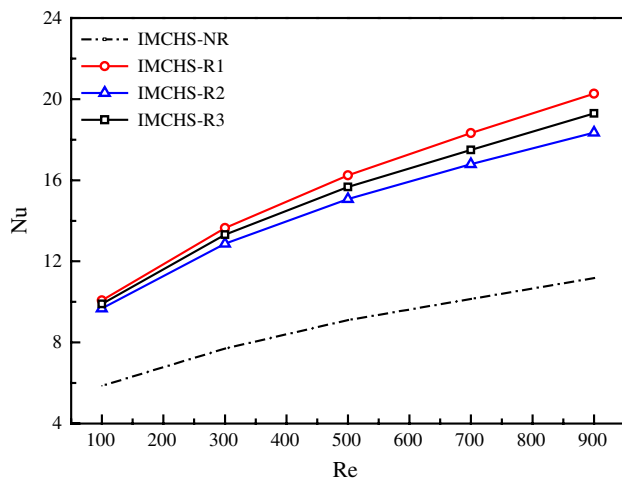


Fig. 10 Average Nusselt number versus Re for the IMCHS with different shaped ribs

chamfer rib presents lower increase in heat transfer and friction than rectangle rib. The decrease in heat transfer is much lower than the decrease in the pressure drop for R3. However, the decrease in heat transfer is much higher than the decrease in pressure drop for R2.

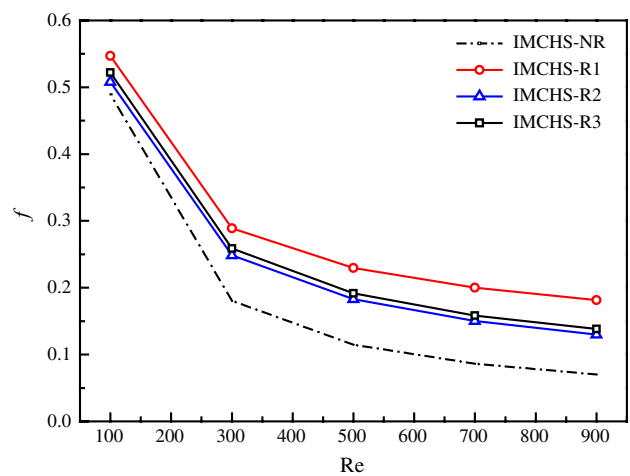


Fig. 11 Average friction factor versus Re for the IMCHS with different shaped ribs

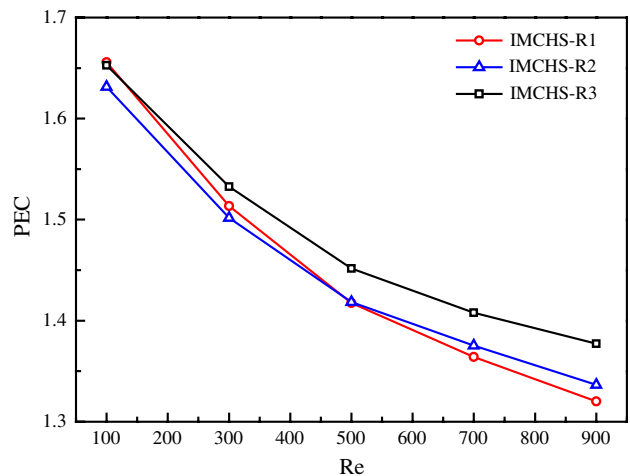


Fig. 12 Average PEC versus Re for the IMCHS with different shaped ribs

Conclusions

This study mainly focused on the laminar flow and heat transfer performance in interrupted microchannel heat sink (IMCHS) with no rib (NR), rectangle rib (R1), triangle rib (R2) and trapezoid rib (R3). The IMCHS-NR shows no effect on heat transfer and flow resistance improvement. The IMCHS with ribs shows significant increase in local heat transfer and friction performance at the windward side of the ribs. The average characteristics reveal that the smaller the chamfer of ribs, the larger average heat transfer and friction performance. The maximum increment of Nu and f can reach 1.81 and 2.59, respectively, for the

IMCHS with rectangle ribs. From the overall heat transfer performance (PEC), the PECs of the IMCHS with three kinds of ribs are all above 1.3, for the whole considered Re range. The trapezoidal rib shows the best behavior, with $PEC = 1.65\text{--}1.38$ in the Reynolds number ranging from 100 to 900.

Acknowledgements Open access funding provided by Lund University. This study is supported by Natural Science Foundation of China (Grant No. 51476042).

Open Access This article is licensed under a Creative Commons Attribution 4.0 International License, which permits use, sharing, adaptation, distribution and reproduction in any medium or format, as long as you give appropriate credit to the original author(s) and the source, provide a link to the Creative Commons licence, and indicate if changes were made. The images or other third party material in this article are included in the article's Creative Commons licence, unless indicated otherwise in a credit line to the material. If material is not included in the article's Creative Commons licence and your intended use is not permitted by statutory regulation or exceeds the permitted use, you will need to obtain permission directly from the copyright holder. To view a copy of this licence, visit <http://creativecommons.org/licenses/by/4.0/>.

References

- Jang D, Yook S-J, Lee K-S. Optimum design of a radial heat sink with a fin-height profile for high-power LED lighting applications. *Appl Energy*. 2014;116:260–8.
- Kandasamy R, Wang X-Q, Mujumdar AS. Transient cooling of electronics using phase change material (PCM)-based heat sinks. *Appl Therm Eng*. 2008;28:1047–57.
- Bahiraei M, Heshmatian S, Keshavarzi M. Multi-attribute optimization of a novel micro liquid block working with green graphene nanofluid regarding preferences of decision maker. *Appl Therm Eng*. 2018;143:11–21.
- Bahiraei M, Heshmatian S. Optimizing energy efficiency of a specific liquid block operated with nanofluids for utilization in electronics cooling: a decision-making based approach. *Energy Convers Manag*. 2017;154:180–90.
- Bahiraei M, Heshmatian S. Electronics cooling with nanofluids: a critical review. *Energy Convers Manag*. 2018;172:438–56.
- Xie G, Li Y, Zhang F, Sundén B. Analysis of micro-channel heat sinks with rectangular-shaped flow obstructions. *Numer Heat Transf A Appl*. 2016;69:335–51.
- Akbari OA, Khodabandeh E, Kahbandeh F, Toghraie D, Khalili M. Numerical investigation of heat transfer of nanofluid flow through a microchannel with heat sinks and sinusoidal cavities by using novel nozzle structure. *J Therm Anal Calorim*. 2019;138:737–52.
- Arappour A, Karimipour A, Toghraie D, Akbari OA. Investigation into the effects of slip boundary condition on nanofluid flow in a double-layer microchannel. *J Therm Anal Calorim*. 2018;131:2975–91.
- Heydari A, Akbari OA, Safaei MR, Derakhshani M, Alrashed AAAA, Mashayekhi R, Ahmadi Sheikh Shabani G, Zarringhalam M, Nguyen TK. The effect of attack angle of triangular ribs on heat transfer of nanofluids in a microchannel. *J Therm Anal Calorim*. 2018;131:2893–912.
- Mohd-Ghazali N, Estellé P, Halelfadl S, Maré T, Siong TC, Abidin U. Thermal and hydrodynamic performance of a micro-channel heat sink with carbon nanotube nanofluids. *J Therm Anal Calorim*. 2019;138:937–45.
- Keshavarz F, Mirabdollah A, Bayat H. Numerical analysis of effect of nanofluid and fin distribution density on thermal and hydraulic performance of a heat sink with drop-shaped micropin fins. *J Therm Anal Calorim*. 2019;135:1211–28.
- Bahiraei M, Heshmatian S. Thermal performance and second law characteristics of two new microchannel heat sinks operated with hybrid nanofluid containing graphene–silver nanoparticles. *Energy Convers Manag*. 2018;168:357–70.
- Wang H, Chen Z, Gao J. Influence of geometric parameters on flow and heat transfer performance of micro-channel heat sinks. *Appl Therm Eng*. 2016;107:870–9.
- Ahmed HE, Ahmed MI. Optimum thermal design of triangular, trapezoidal and rectangular grooved microchannel heat sinks. *Int Commun Heat Mass Transf*. 2015;66:47–57.
- Xie G, Shen H, Wang C-C. Parametric study on thermal performance of microchannel heat sinks with internal vertical Y-shaped bifurcations. *Int J Heat Mass Transf*. 2015;90:948–58.
- Chai L, Xia G, Zhou M, Li J, Qi J. Optimum thermal design of interrupted microchannel heat sink with rectangular ribs in the transverse microchambers. *Appl Therm Eng*. 2013;51:880–9.
- Wong K-C, Lee J-H. Investigation of thermal performance of microchannel heat sink with triangular ribs in the transverse microchambers. *Int Commun Heat Mass Transf*. 2015;65:103–10.
- Chai L, Xia GD, Wang HS. Laminar flow and heat transfer characteristics of interrupted microchannel heat sink with ribs in the transverse microchambers. *Int J Therm Sci*. 2016;110:1–11.
- Mehta SK, Pati S. Analysis of thermo-hydraulic performance and entropy generation characteristics for laminar flow through triangular corrugated channel. *J Therm Anal Calorim*. 2019;136:49–62.
- Wang W, Zhang Y, Li B, Li Y. Numerical investigation of tube-side fully developed turbulent flow and heat transfer in outward corrugated tubes. *Int J Heat Mass Transf*. 2018;116:115–26.
- Mashayekhi R, Khodabandeh E, Akbari OA, Toghraie D, Bahiraei M, Gholami M. CFD analysis of thermal and hydrodynamic characteristics of hybrid nanofluid in a new designed sinusoidal double-layered microchannel heat sink. *J Therm Anal Calorim*. 2018;134:2305–15.
- Sundén B. *Introduction to heat transfer*. Ashurst: WIT Press; 2012.
- Wang W, Zhang Y, Lee K-S, Li B. Optimal design of a double pipe heat exchanger based on the outward helically corrugated tube. *Int J Heat Mass Transf*. 2019;135:706–16.
- Menni Y, Azzi A, Chamkha A. Enhancement of convective heat transfer in smooth air channels with wall-mounted obstacles in the flow path. *J Therm Anal Calorim*. 2019;135:1951–76.
- Pishkar I, Ghasemi B, Raisi A, Aminossadati SM. Numerical study of unsteady natural convection heat transfer of Newtonian and non-Newtonian fluids in a square enclosure under oscillating heat flux. *J Therm Anal Calorim*. 2019;138:1697–710.

Publisher's Note Springer Nature remains neutral with regard to jurisdictional claims in published maps and institutional affiliations.